Sperm-Micromotors for Cargo-Delivery through Flowing Blood

Haifeng Xu[1,2], Mariana Medina-Sánchez[1*], Manfred F. Maitz[4], Carsten Werner[4] and Oliver G. Schmidt[1,2,3]*

[1]Institute for Integrative Nanosciences, Leibniz IFW Dresden, Helmholtzstraße 20, 01069 Dresden, Germany

[2]Research Center for Materials, Architectures and Integration of Nanomembranes (MAIN), Rosenbergstraße 6, TU Chemnitz, 09126 Chemnitz, Germany

[3]School of Science, TU Dresden, 01062 Dresden, Germany

[4]Max Bergmann Center of Biomaterials, Leibniz Institute of Polymer Research Dresden, Dresden, 01069, Germany

*Corresponding author e-mail: h.xu@ifw-dresden.de; m.medina-sanchez@ifw-dresden.de

ABSTRACT

Micromotors are recognized as promising candidates for untethered micromanipulation and targeted cargo-delivery in complex biological environments. However, their feasibility in the circulatory system has been limited due to the low thrust force exhibited by many of the reported synthetic micromotors, being not sufficient to overcome the high flows and complex composition

of blood. Here we present a hybrid sperm-micromotor which can actively swim against flowing blood (continuous and pulsatile) and perform the function of heparin cargo-delivery. In this bio-hybrid system, the sperm flagellum provides a high propulsion force while the synthetic microstructure serves for magnetic guidance and cargo transport. Moreover, single sperm-micromotors can assemble into a train-like carrier after magnetization, allowing the transport of multiple sperm or medical cargoes to the area of interest, serving as potential anti-coagulant agents to treat blood clots or other diseases in the circulatory system.

KEYWORDS

sperm-micromotors, blood stream, cargo-delivery, heparin, rheotaxis, anti-coagulation

On the way to the next generation of medical treatments, biomedical micromotors are attracting a lot of attention due to their controllable motion, their minimal invasiveness, and their versatility for diverse biochemical functions.[1] Moreover, equipped with specific propulsion mechanisms (*e.g.* by local chemical reactions,[2] remote acting forces[3] or motile bio-organisms[4]), micromotors can perform various operations with high precision such as targeted drug delivery,[1] microsurgery[5–8] and sensing,[9,10] to mention some of them. Surprisingly, as the most common administration route, the blood circulation system, has only rarely been explored as a transportation route for micromotors. Among the few attempts, catalytic microjet engines were shown to swim in H_2O_2 solution containing ten times diluted red blood cells under static conditions. The results suggested that catalytic engines prepared by rolled-up and electrodeposition methods exhibited motion only in highly diluted dispersions of red blood cells and serum, probably due to the high viscosity of the whole blood as well as clogging produced by red blood cells.[11,12] Magnetically-driven micro-

helices were also actuated in static blood dilutions, observing a stick-and-slip motion, which was related to the colloidal jamming of blood cells. These micromotors were chemically stable and biocompatible in blood thanks to their ferrite coating.[13] Another attempt was made by using $CaCO_3$ microparticles as potential hemostatic agents.[14] Unlike the first two cases where micromotors moved in static blood solutions, $CaCO_3$ microparticles swam against blood velocity up to 5.9 mm/s by the propulsion of locally generated CO_2 bubbles, though with only random motion due to the lack of a guidance mechanism. However, the above-mentioned self-propelled particles and microengines were driven by toxic fuels like H_2O_2 or acidic substances, being distant from any medical treatment in living organisms. Another strategy has been to turn red blood cells (RBCs) into micromotors. Wu *et al.* functionalized RBCs with magnetic particles for guidance while propelling them with acoustic waves. The experiments in this work were focused on studying the stability of RBCs micromotors under acoustic waves, but experiments under flow conditions showing a specific function of cargo release were not shown in this work.[15] More recently, Khalil, *et al.*, reported a 2 mm helical robot able to perform mechanical rubbing of blood clots in *in vitro* and *ex vivo* models containing PBS buffer against a flow of *ca.* 10 mL/h, which corresponds to a blood velocity of 0.22 mm/s (considering a vessel diameter of 4 mm).[16] The flow in this work was similar to that of small arterioles, capillaries, and venules. However, the operation of micromotors under more realistic blood stream conditions remain a challenge due to the high complexity of the blood fluid and its high flow rates in the circulatory system. Besides, blood contains a variety of macro- and small molecules which can influence the motion and function of any medical micromotor.[17] Blood pH is another factor which is regulated in a narrow range between 7.35 and 7.45, thus any modification of the blood composition by adding other substances for fueling the micromotors would be harmful in any further realistic application.[18] Half of the whole blood is

constituted by different cell types, including 5×10^9 red blood cells/mL,[17] which would continuously interfere with the micromotors mobility, consuming a lot of energy in the process. Another aspect is the exposure of micromotors to the innate immune system in blood, which would eliminate them by *e.g.* phagocytosis,[19] or when the micromotors size is too small (<5 µm).[20,21]

To overcome the abovementioned hurdles, sperm-based micromotors seem promising to our view. They hold several advantages such as their powerful propulsion generated by the beating of the sperm flagella. Sperm are also able to swim for several days with a drag force up to 100 pN,[22]comparable to the propulsion force reported by some of the most powerful catalytic micromotors (ranging from 3.77 pN to 500 pN).[23,24] The most important feature of sperm-micromotors to operate in the blood stream is their ability to swim against flow (rheotaxis) as well as close to boundaries (thigmotaxis), where the blood velocity is lower than the average one, due to shear stress, being the most efficient guidance mechanisms for sperm to reach the oocyte when accomplishing their natural function,[25] Additionally, in combination with a synthetic magnetic scaffold, sperm-micromotors can be precisely guided and operated by an external magnetic field to further release a cargo at the right place and time by making use of cutting-edge imaging techniques.[26,27] The horn-like cap not only allows the assembly with other microcaps for multiple sperm transport but also serves as an anchoring structure, holding the sperm-micromotor's position under strong blood velocity when it is forced to point towards the channel surface by means of an external magnetic field. The cap was designed to reduce the drag forces allowing it to squeeze through the blood cells and within heterogeneous fluids. Regarding the safety of sperm-based micromotors, sperm offers unique advantages that other exogenous materials (*e.g.* synthetic cargoes, bacteria, viruses) do not have. For example, it shares the same type of membrane composition with other body cells, ensuring their adaptability. Sperm does not proliferate or secret

any harmful bio-substances.[28] Besides, specific proteins (*e.g.* CD59, decay-accelerating factors and membrane cofactor proteins)[29] are expressed on the sperm membrane to inhibit body inflammation. Sperm also owns a unique extracellular organelle (prostasome)[30] to suppress the local immunoreactions. It is also worth noting that phagocytosis of the granulocytes is highly dependent on the target size. For example, objects of 3 µm in diameter face the risk of phagocytosis by macrophages as reported in the literature.[20] Sperm has a length over 50 µm and even the head is already ~5 µm wide. Regarding the synthetic component, it can be fabricated with biodegradable materials,[31] and coatings such as polyethylene glycol[32] or cell-membrane camouflages[33] to avoid the clearance by the immunological system during the treatment period as reported before in the literature.

Sperm-micromotors have been already shown in particular to assist sperm with motion deficiencies to reach the oocyte,[34,35] for delivering nanomedicines,[36] anticancer drugs to treat gynecological cancers,[37,38] or other organic/inorganic payloads.[39,40] In this work, we present streamlined-horned caps (SHCs) hybrid sperm-micromotors (**Figure 1**), which can efficiently and controllably swim against flowing blood. As a proof-of-principle of a potential medical use, we functionalize the microcaps with heparin-loaded liposomes to realize a localized anticoagulant function. This study not only initiate application scenarios for micromotors in the circulatory system, but envisions an administration route of sperm or sperm-hybrid micromotors for future local medical applications.
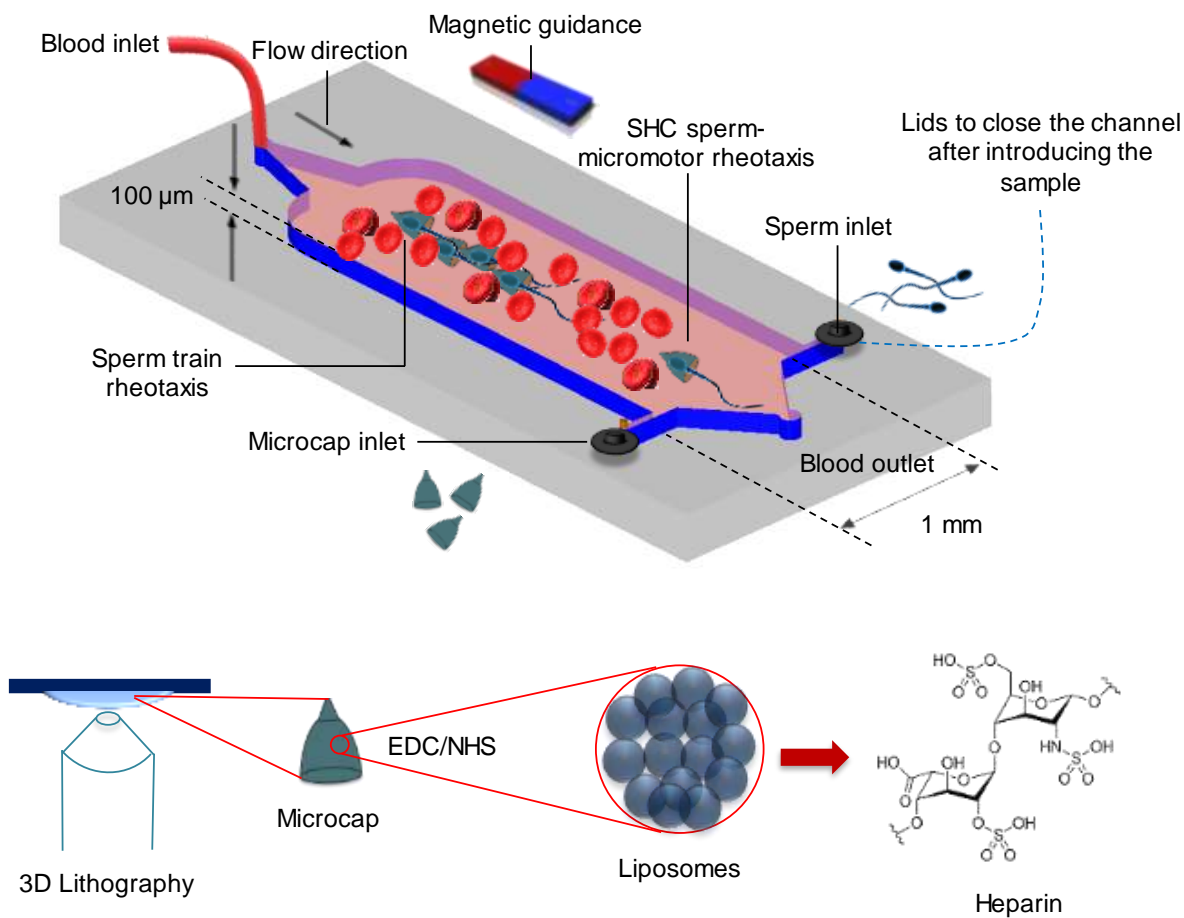
Fig. 1. Concept of the blood-adapted SHC sperm-micromotors.

RESULTS AND DISCUSSION

SHC sperm-micromotors in blood. Different to other *in vivo* applications, any medical mission

in blood faces a particularly complicated working environment, including the presence of various

substances and cells, complex hemorheological properties, and high flows. In order to efficiently

design and manufacture a sperm-micromotor, we first ran flow simulations and compared the

hydrodynamic characteristics of two different designs, a tubular and a streamline-horned cap

(SHC) with the same diameter (13 µm) and height (15 µm). **Figure 2a, i-ii** shows the relative

pressure on both cap designs when subjected to an aqueous solution containing solid spheres of about 5 µm diameter (mimicking red cells) (more details in the **Experimental section and Supporting Information (Figure S1)**). As expected, the tubular cap is obstructed by the spheres-mimicking cells on its front surface with a high static pressure. In contrast, the shape of the SHC facilitates the passing of the sphere-mimicking cells forming a stable wake flow around it. At a swimming speed of 50 µm/s, the energy loss (defined as the generated heat per unit time) of the SHC is about 53% of the tubular cap one.

To verify the performance of both designs, the microcaps were fabricated by two-photon lithography (SEM images of the SHC are shown in **Figure 2b**), followed by the coating of Fe, Ti and SiO$_2$ nanofilms for both magnetic guidance and biocompatibility. Subsequently, microcaps were mixed with sperm and added into 4× diluted whole blood. We used bovine sperm as model for our experiments as their morphology is similar to human sperm.[37] Furthermore, it is worth noting that the whole sperm-cap assembly was smaller than the venules size (*ca.* 30 to 100 µm in diameter) - intended operating location. In further studies with human sperm, microcaps will be fabricated with an even smaller diameter of ca. 5 µm than the current one (*ca.* 15 µm), being in the size range of the thinnest blood capillaries (*ca.* 5-10 µm diameter). After introducing sperm, we observed that free sperm swimming in blood retained an average speed of 76 ± 17 µm/s (n = 17), comparable to the one in sperm medium (89 ± 14 µm/s, n = 30). However, due to the obstructing blood cells and the lack of guidance, freely swimming sperm in 2× blood tended to swim on circular trajectories forming hollow regions from where the sperm were not able to escape (see **Figure 2c, i** and **Video S1**). When swimming in confined space, such as the oviduct, sperm tend to swim near the walls (thigmotaxis), displaying circular or curvilinear trajectories due to the chirality of the flagellar beating. The asymmetric beating of the flagellum pushes the nearby blood

cells out of the swimming area. As more and more cells are pushed close to each other, the cells form a dense boundary wall, trapping sperm inside the formed pool. For that reason, the use of a synthetic component, in particular a magnetic cap, serves as a guidance vehicle for sperm to ensure the controllable delivery of therapeutic cargoes at the desired location by applying an external magnetic field. As an example, **Video S2** shows the coupled SHC sperm-micromotors, where the coupling efficiency of sperm and microcaps was *ca.* $62 \pm 19\%$ (n = 6) with respect to the total amount of microcaps. In this case, the sperm concentration was 3×10^4 sperm /µL and the number of microcaps was 100 caps/µL.

In agreement with the hydrodynamic simulations, the magnetic tubular sperm-micromotors could not swim in 4× diluted blood for a long period of time due to the heavy load created by the stacked blood cells on the flat front side of the microtubes, as shown in **Figure 2c, ii**. In contrast, SHC sperm-micromotors swam more efficiently thanks to the streamlined-horn front which easily squeezed through the blood cell crowd (see **Figure 2c, iii, 2d** and **Video S3** for details). In this way, blood cells were pushed aside, passing by in the vicinity of the cap wall forming a broad wake flow behind the SHC (see **Video S4** for details). From 8× to 2× diluted blood, the swimming velocity of the SHC sperm-micromotors continuously decreased as shown in **Figure 2e**.

SHC sperm-micromotor in flowing blood. Some of the barriers that micromotors have to face to operate in the blood stream are the high fluid velocities and the presence of a large number of cells. The physiological blood velocity in microcirculation (particularly in the venules) is *ca.* 0.4 mm/s.[41] This number decreases to *ca.* 0.15 mm/s at disease sites when suffering for example embolism.[42,43] Thus, micromotors have to overcome the hitting of blood cells and the resistance from the serum flow at a high velocity. To investigate the swimming capability of SHC sperm-micromotors, we used polydimethylsiloxane (PDMS) microfluidic chips to mimic microvessels

with a cross section of *ca.* 0.4 mm^2, and imposed a continuous or pulsatile flow using a syringe pump for the experiments. Firstly, sperm-micromotors were introduced into the microfluidic channel containing 2× diluted blood under a blood velocity of 0.167 mm/s to verify their magnetic response and the possibility to guide them in such complex conditions (**Figure 3a, Video S4**). Then, by maintaining the permanent magnetic field at a fixed orientation along the microchannel, and keeping the blood velocity at 0.167 mm/s, we evaluated the rheotaxis capability of the sperm-cap assembly and we observed a similar behavior of the sperm-micromotors swimming against the flow as compared to free swimming sperm (see **Video S5**). In the natural case, sperm reorient in fluid flow to align against the flow direction and swim upstream through the oviduct channel. This process is still not well understood and there are contradictory hypotheses where rheotaxis is explained as a purely physical phenomena, or as an active process where the fluid flow is sensed by sperm mechanosensitive channels. Recent studies suggest that no significant difference exists in both flagellar beating and released Ca^{2+} ions between rheotaxis and freely swimming sperm, indicating that it is mainly a hydrodynamic effect between the sperm flagellum and its surrounding fluid flow.[44] Based on our experiments, the same concept applies to the sperm-micromotor, probably because the flagellar beating of the coupled sperm is not affected by the cap as it was designed with a large opening and size which fits to the sperm head, allowing for full amplitude sperm beating (**Figure 3b**).
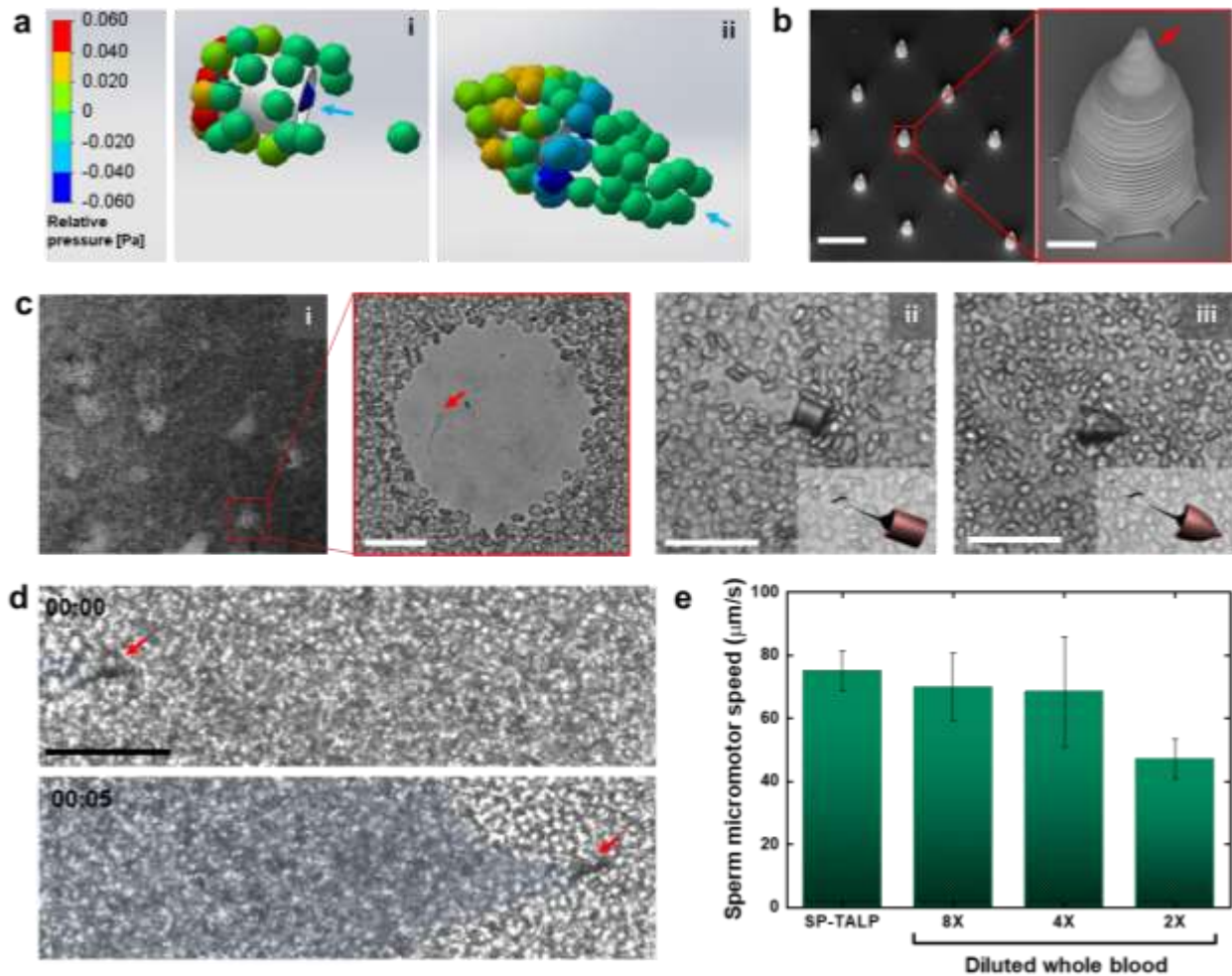
Fig. 2. (a) Hydrodynamic simulations of (i) tubular and (ii) SHC caps, assuming a swimming speed of 50 µm/s, and particles mimicking red blood cells of 5 µm in diameter. Blue arrows point at the swimming direction. (b) SEM images of SHCs. The red arrow indicates the horn structure used for enhancing the micromotor motion in blood. Scale bars: 40 µm in the left panel and 5 µm in the right panel with higher magnification. (c) (i) Free sperm moving in 2× diluted blood; Sperm-micromotors with (ii) a tubular and (iii) a SHC cap in static 8× blood solution. Scale bars: 40 µm. (d) Image sequence of a SHC sperm-micromotor moving in static 2× blood. Transparent blue region indicates the wake flow resulting from their motion. Scale bar: 40 µm. (e) Speed

comparison of SHC sperm-micromotors varying with the dilution of whole blood and sperm medium, n = 4.

By increasing the fluid velocity, sperm-micromotors also lower their rheotaxis speed until reaching a critical blood velocity where the speed of the sperm-micromotor decreases down to 0 µm/s. If the blood velocity exceeds the tolerance limit of the sperm-micromotor speed, the sperm is not able to swim further and instead is dragged into the direction of the blood velocity (see **Figure 3c**). **Figure 3d, i** depicts the absolute sperm-micromotor speed as a function of the blood velocity. When the sperm-micromotor speed decreases down to 0 µm/s, blood velocity is around 0.175 mm/s, being equivalent to its rheotactic speed under continuous flow. This value is higher than the swimming speed in static blood due to the wall stress shear gradient which facilitates the progression of sperm. Sperm can also generate stronger thrust force in the presence of a load (fluid resistance), as previously reported for flagellated *Chlamydomonas cells*.[45] Additionally, sperm-micromotors are expected to swim even against higher flow velocities when using channels with larger cross sections. However, in our experiments we used 100 µm thick microchannels to avoid difficulties visualizing and tracking sperm-micromotors through the dense blood cells.

To explore the influence of continuously changing blood velocity on the swimming performance of sperm-micromotors, we defined a sequence of linearly increasing flow veloctiy by using a syringe pump over a time period of 80 s, increasing the blood velocity up to the maximum and decreasing it again to the original value (see **Materials and Methods Section and Video S6**). As anticipated, the sperm-micromotor moves forward at decreasing speeds upon the increase of the blood velocity (**Figure 3d, ii**). Then, after reaching the threshold fluid velocity, the sperm thrust force cannot overcome the fluid drag force, and the sperm-micromotor is displaced along with the fluid into the direction of the flow. If the flow decreases again, the sperm-micromotor recovers its

speed but with a slightly lower magnitude, probably due to the sperm energy consumption over time and the previously imposed flow load (**Figure 3d, ii** and **Figure S2**).

Blood circulation in the human body is mainly caused by two powerful driving forces: the heart beat for arterial ejection,[46] and the muscle pump for venous and capillary returns.[47] The periodicity of the muscle pump depends on the rhythm of the muscular movement. In view of this, we programmed the pulsing perfusions to observe the adaptability of the sperm-micromotor in periodically changing blood velocity. We set the impulse cycle as 3 s to mimic the rhythm of blood return by the respiratory muscle pump under quiet breathing conditions.[48] **Figure 3e, i** shows the forward displacement when the sperm-micromotors swim against pulsing blood velocity at a velocity of 0.125 mm/s. In 8 cycles of perfusions (24 s), the sperm-micromotors progressed forward over a distance of about $596 \pm 43\,\mu$m in total. The increasing displacement fluctuated with the pace of the perfusing pulsation. We also programmed a stronger pulsing flow at 0.208 mm/s. Although the sperm-micromotor could barely progress forward when the perfusion was on, it could still speed up very fast and continue moving in between two perfusions (**Figure 3e, (ii)** (example videos can be seen in **Video S7**). Moreover, we found a ratchet brake mechanism that could help the sperm-micromotor swim against higher pulsing flows. In this case, the sperm-micromotors were first guided towards the wall and forced to constantly swim near the substrate. Due to the preference of the sperm to move near surfaces, the sperm-micromotor can swim forward parallel to the substrate when the flow is off. When the flow is on, the sperm starts swimming against it (rheotaxis) until the flow rate reaches the threshold value in which the sperm is not able to swim forward (see **Figure 3f**). After that, sperm is not able to hold its head upstream and thus the sperm-micromotor is reoriented by the magnetic field until the horn in the engineered cap gets in contact with the channel surface, serving as an anchor. The sperm-micromotor can therefore hold its

position under strong flow. When the flow decreases again, the sperm-micromotor recovers its swimming speed and successfully progresses until the next flow peak is reached. As depicted in **Figure 3f, iii**, the flow impact was at that moment counterbalanced by the induced static friction between the top horn of the sperm-micromotor and the substrate. **Video S8** shows that sperm-micromotors could resist high flow velocities (up to 0.833 mm/s) when implementing the ratchet break mechanism, progressing when the perfusion is turned off (in pulsatile blood flow mode).
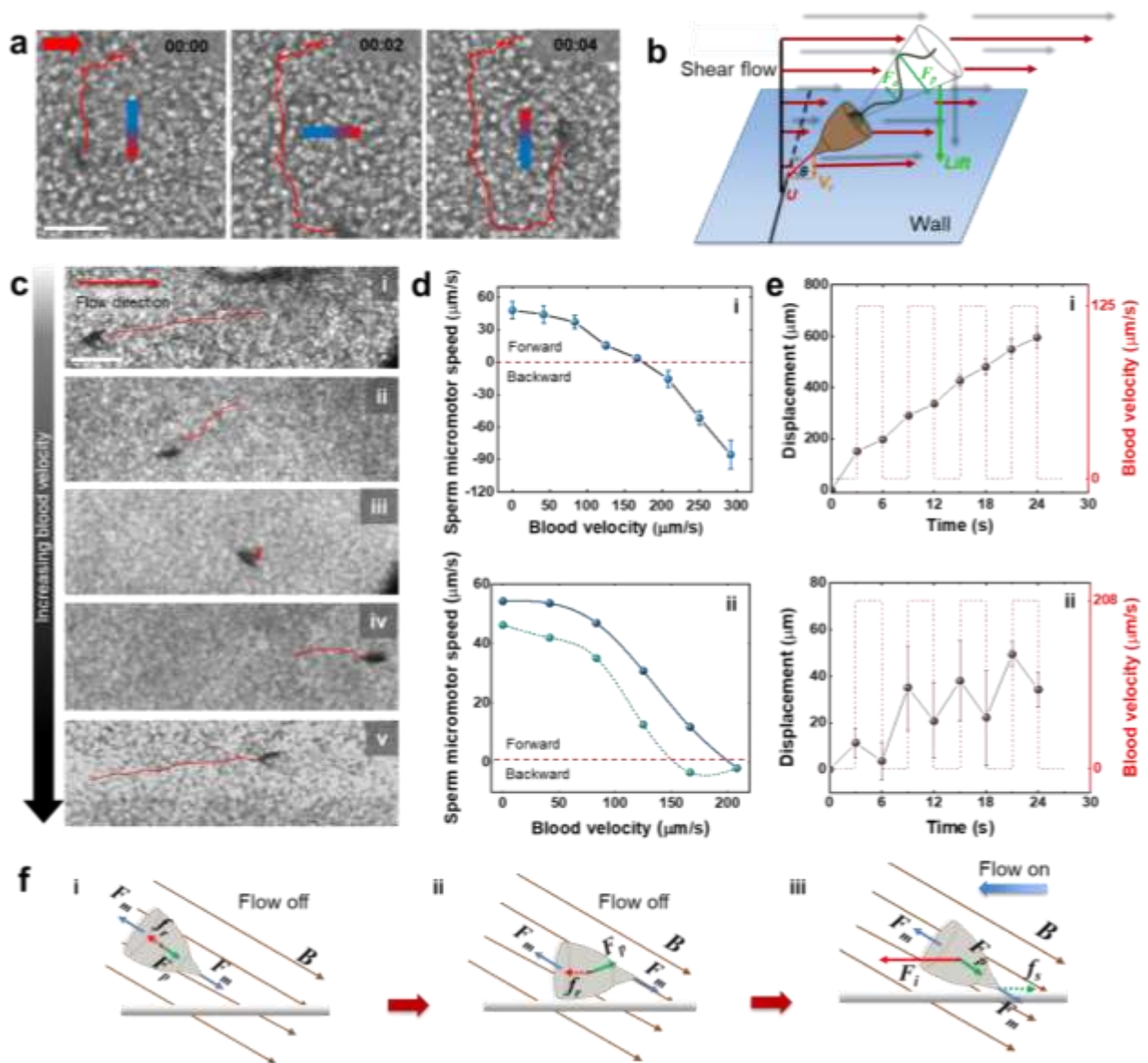
Fig. 3. (a) Magnetic guidance of a SHC sperm-micromotor swimming against blood velocity of 0.167 mm/s. (b) Rheotaxis of the sperm-micromotor resulting from the chiral beating and imbalance of hydrodynamic force on posterior (F_p) and anterior flagellum (F_a). When $F_p > F_a$, a net lift force is generated on the flagellum, perpendicular to the flow direction. The lift force provides the sperm-micromotor a rheotactic velocity (V_r) toward the wall, leading to a total swimming speed (U) at an angle (θ) to the horizontal direction. (c) Track of SHC sperm-micromotors against continuous flowing 2x blood at a velocity of (i) 0.042; (ii) 0.125; (iii) 0.167; (iv) 0.208; (v) 0.292 mm/s. The duration of the tracking in all cases was 3 s. (d) Absolute swimming speed of SHC sperm-micromotors *versus* 2x blood velocity. (i) Sperm-micromotor speed against varying blood velocity (n = 4); (ii) Hysteresis loop of SHC sperm-micromotor speed against continuously changing blood velocity. (e) SHC sperm-micromotor swimming against pulsing blood velocity at (i) 0.125 mm/s; (ii) 0.208 mm/s. (n = 4). (f) Schematic of the ratchet brake mechanism: (i) Guiding the sperm-micromotor toward the substrate; ii). Sperm-micromotor swimming without flow; (iii) Ratchet brake against flow. F_m: magnetic torque. F_p: sperm propulsion. f_r: hydrodynamic resistance. F_i: blood velocity impact. f_s: static friction. Scale bars: 40 µm.

The swimming height of the sperm-micromotors was measured by microscopy with a high-precision motorized z plane focusing stage (**Video S9**). When the perfusion of 2× diluted blood was turned on, the sperm-micromotors tended to swim against flow (rheotaxis) and near to the bottom wall of the channel (thigmotaxis). Then we focused on top of the SHC cap during the sperm-micromotor motion in order to distinguish it from the surrounding cells. The focal distance between the top of the microcap and the substrate was measured to be *ca.* 21 µm, resulting in a swimming height of the micromotor of *ca.* 8 µm, after subtracting the diameter of the microcap

(13 µm). Such separation distance might be due to a blood cell monolayer underneath the micromotor. Besides, the lift force from the substrate created by the tail beating and the flow also might have an influence on the above separation distance.

As the linear blood velocity differs with the relative distance to the channel wall due to the shear stress, it is important to know the *in-situ* blood velocity that the sperm-micromotor should overcome when swimming upstream. We performed fluid dynamics simulations by using SolidWorks to determine the flow profile considering the dimensions of the channel, material, and roughness (**Figure S3, S4**). We found that when an average blood velocity is set at ~0.175 mm/s, the blood velocity near the wall surface (8 µm) was only *ca.* 0.070 mm/s, lower than the average blood velocity, as expected. To correlate the computational velocity with the experimental result, we performed the tracking of uncoupled caps moving along with the blood stream. The measured cap dragging velocity was *ca.* 0.036 mm/s, being *ca.* 2 times smaller than the one obtained by simulation. The discrepancy between these two values comes from the fact that in the simulation, the probe size and the corresponding involved forces (*e.g.* electrostatic and drag forces) were not considered.

In order to measure the swimming height of the sperm-micromotor in the ratchet brake mechanism, we forced the sperm-micromotor to point towards the bottom surface by means of an external magnetic field. As shown in **Video S9**, the focusing plane was fixed on the horn of the sperm-micromotor to observe its anchor-like function. In this mechanism with an averaged blood velocity of 0.833 mm/s, the sperm-micromotor remained at a height of ~3 µm (with no cell monolayer underneath the sperm-micromotors). Thus, sperm-micromotor would be able to swim against a blood velocity of *ca.* 0.169 mm/s (based on simulation) or *ca.* 0.104 mm/s (based on measurement) *in situ*, meaning ~3 µm distance away from the wall. Rheotaxis/thigmotaxis inherited from the

sperm and the ratchet brake mechanism from the coupled horned-cap facilitate the sperm-micromotor to swim against higher blood velocity.

Sedimentation acts as another possible factor obstructing sperm-micromotors. In our experiments, blood samples were agitated right before perfusion. Every run was less than 20 min. No obvious sedimentation of 2× diluted blood was observed in the microchannels during this period of time. Mainly driven by gravity, blood sedimentation can be seen more clearly at low concentration of blood cells.[49] In order to evaluate the influence of cell density at different heights on the swimming behavior of sperm-micromotors, we introduced 10× diluted blood in 1 mm thick microchannel and waited 0.5 h. Sperm-micromotors were magnetically guided to different heights for observation. As displayed in **Video S10**, the sperm-micromotor can swim progressively at both the bottom (through sediment cells) and top of the channel. When swimming right above the sedimented cells, the sperm-micromotor however cannot resist the same flow perfusion. This could be attributed to the increasing blood velocity away from the channel wall. These findings emphasized again the difficulty of swimming under the blood stream and the advantage of sperm and sperm-micromotors to swim close to the walls and against flow.

SHC sperm-train swarm in flowing blood for multiple cargo delivery. As a step beyond single sperm-micromotor guidance, we employed a different coating strategy to induce the self-assembly of multiple sperm-micromotors into a train-like configuration. This was achieved by depositing Fe at a 75° angle (details are given in the **Materials and Methods section**). **Figure S5** shows a schematic of the SHCs assembling into a sperm-train. When a uniform magnetic field is applied across the sample with randomly dispersed SHCs and sperm, the magnetic layer on each SHC acquires a dipole configuration, leading to the alignment of SHCs along the direction of the

magnetic field. The dipole-dipole based long-range attraction between two different SHCs results in their self-assembly. **Figure 4a** shows the change of the magnetic field distribution from a single SHC to a 4-SHC sperm-train. A more stable field distribution is found after the assembling process, mainly caused by the horn of the caps as anchor points within the sperm train. The assembled "train" can be further prolonged, stretched and organized with more and more SHCs involved under the alignment of the magnetic field (see **Figure 4b**), similar to the assembling process of previously reported microcubes[50] and microparticles.[51] The assembling of SHCs can be improved even more by decreasing the distance between them (by stirring or by increasing the density of caps in the solution). **Figure 4c** shows a sperm-train with 9 SHCs and 7 sperm. The SHCs are periodically arranged into opposite directions of the sperm-train, which ensures that the beating of the sperm flagellum in one SHC is not disturbed by another, also facilitating the sperm coupling to the structures. **Video S11** shows the guided locomotion of the sperm-train in sperm medium. During the guidance, the sperm-train is still capable to assemble with other sperm-trains, breeding a new longer sperm-train but with a lower swimming speed. Finally, when the sperm-train arrives at the desired position, we can easily trigger the coupled sperm to escape by repeatedly flipping the SHCs and dissembling the sperm-train by abruptly turning the magnetic field. In this way, the SHCs are precisely transported and accumulated at the desired position. 4× diluted whole blood was used as a model environment to verify the swimming performance of the sperm-train for further blood application. As shown in **Figure 4d**, various sperm-trains with different numbers of SHCs are assembled and swim in static blood fluid (see also in **Video S12**). The guidance can be performed not only on a single sperm-train, but also on a troop of collective sperm-trains and sperm-micromotors as can be seen in **Figure 4d**. The swimming performance of sperm-trains in static blood solution is depicted in **Figure 4e**. The average swimming speed generally decreases

with the increase of the SHCs numbers in sperm-trains. The cap number dependent swimming performance shows the same behavior when the sperm-trains swim against flow. For example, as tracked in **Figure 4f**, the average swimming speed of a 4-SHCs sperm-train against a blood velocity of 63 µm/s was 32 µm/s, while a single SHC sperm-micromotor could swim at a high speed of 97 µm/s. This speed decrease is probably because sperm are not pushing the cargoes in a synchronized way. The interference between the traveling waves generated by the tail beating of the coupled sperm as well as the increased load (caps number) could also influence the speed. In order to obtain a better understanding of the interaction between sperm micromotors within a sperm-train, further modeling and experiments are required.
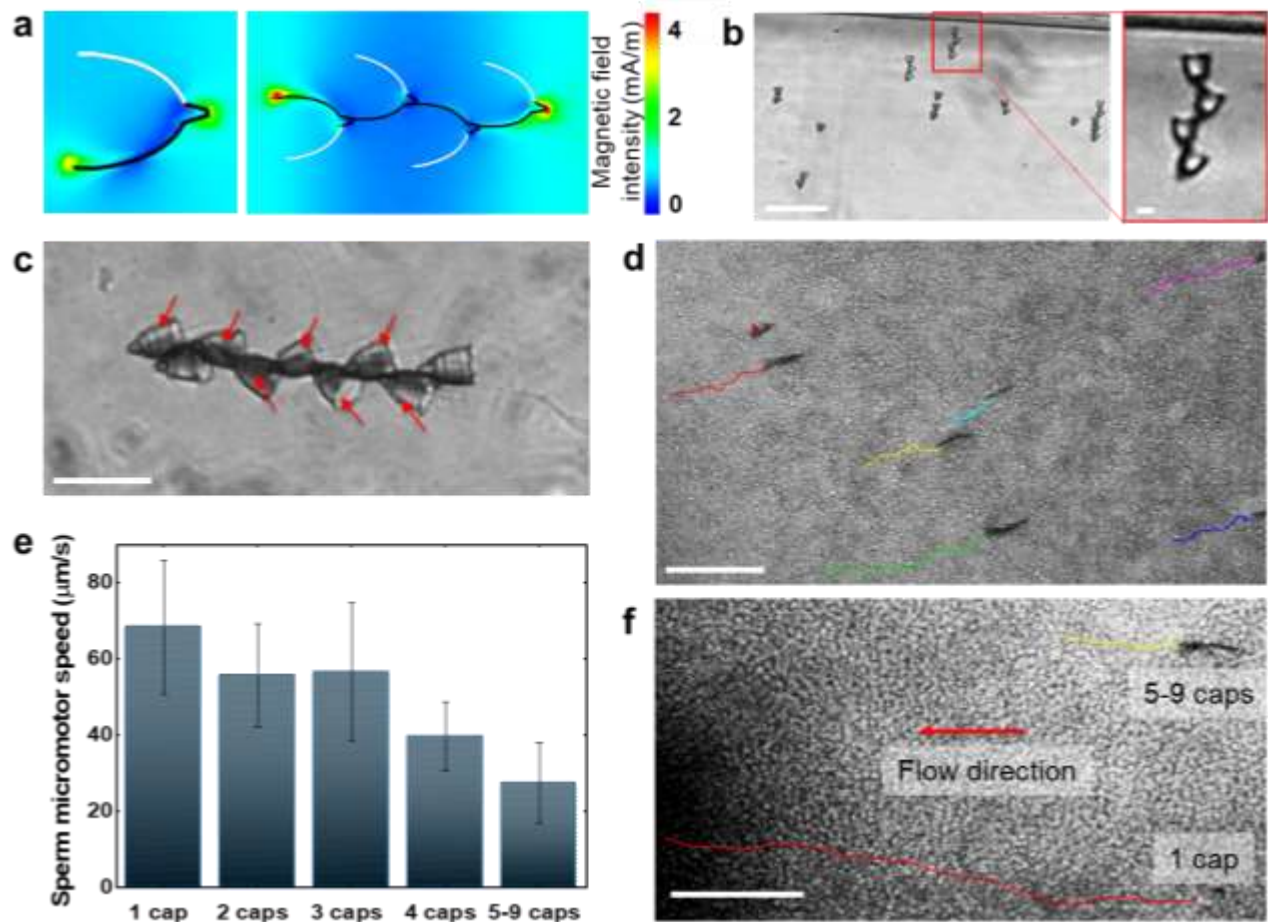
Figure 4. (a) Magnetization simulations of a SHC and a 4-SHC sperm-train, both with partial iron coating. The metal coated part is colored in black. (b) Alignment of assembled SHCs without sperm. (c) A sperm-train swimming in sperm medium (SP-TALP). Red arrows point at the sperm heads. (d) A troop of sperm-trains swimming in 4× diluted blood. (e) Swimming speed of sperm-trains vs cap number. (n = 6). (f) Track of a sperm-train and a SHC sperm-micromotor swimming against flowing blood. Scale bars: 100 µm.

SHC sperm-micromotor for anti-coagulation application. As a primary demonstration of the potential application of the sperm-micromotor for a chemical medication in blood, we endowed the sperm-micromotor with an anti-coagulation ability. Heparin-loaded liposomes were prepared by the extrusion method (see **Materials and Methods section**) and covalently immobilized onto SHCs by 1-Ethyl-3-(3-dimethylaminopropyl)carbodiimide) (EDC) / *N*-Hydroxysuccinimide (NHS) chemistry. In order to characterize the loading of heparin within the liposomes, Alexa 488-conjugated heparin was used as payload, thus a high fluorescence intensity was detected throughout the liposomes-functionalized SHCs, indicating an intact immobilization compared to the bare SHCs (**Figure 5a**). The SEM images in **Figure 5b** illustrate the distribution and density of liposomes on the SHCs. The size of the liposomes varies from 30 to 150 nm. Since a 100 nm pore size filter membrane was used to control the liposome sizes, the larger liposomes probably originated from liposome fusion during the drying process.[52,53] As illustrated in **Figure S6**, along with the increase of the liposome concentration, the density of liposomes increases into densely packed arrays on the micromotor surface. **Figure S6** also shows the comparison between functionalized and non-functionalized microcaps.

After washing and drying, we re-dispersed the heparin-loaded liposomes, immobilized SHCs (HLSs) in PBS and evaluated the anti-coagulation efficiency of the HLS sperm-micromotor system by determining the activated clotting time (ACT). Noticing the considerable burst release effect,[54] we only re-dispersed the HLSs in PBS right before used. After activation with thrombin, the group treated with free swimming sperm showed a comparable clotting time (95 ± 26 s) to the blank control of 2× diluted whole blood (85 ± 18 s). Bare SHCs (75 ± 26 s) did not show a significant influence on the blood clotting, either, presumably because of the bio-compatible cap coating. No clotting was found in the HLS sperm-micromotor system even after 5 min, demonstrating a high anti-coagulation capability provided by the released heparin. Because of medium evaporation, we did not observe the samples for longer times. **Figure 5c, i-ii** illustrates 8× diluted blood samples differently treated with the HLS sperm-micromotors and the bare SHC sperm-micromotors in microfluidic channels. After 5 min activation, blood samples including bare SHC sperm-micromotors had already been found with fibrin clots, while the samples treated with HLS sperm-micromotors were still clean with well dispersed single blood cells throughout. Furthermore, a whole blood incubation assay was implemented to quantitatively analyze the anti-coagulant activity of HLS sperm-micromotors in human blood. Prothrombin fragment F1+2[55] and integrin CD11b,[56] as markers of the coagulation cascade and granulocyte activation processes, respectively, were determined to evaluate the coagulation and inflammation levels of the treated blood. As shown in **Figure 5d**, the sperm-micromotors induced the lowest F1+2 concentration, while the bare SHCs and sperm samples did not deviate from the blank blood. All groups had commensurate counts of CD11b, which showed that both the SHCs and the sperm did not induce any obvious innate inflammatory response. The significantly lower level of hemostasis activation in the HLS sperm-micromotors group reflected a valuable heparin-induced anti-coagulation effect.

In a real scenario, HLS sperm-micromotors would be propelled and guided near the embolism site, suppress the hemostasis activation by releasing heparin gradually into the environment and consequently prevent blood clots formation. This system could also be further expanded to load various thrombolytic drugs for the therapy of already formed thrombus.
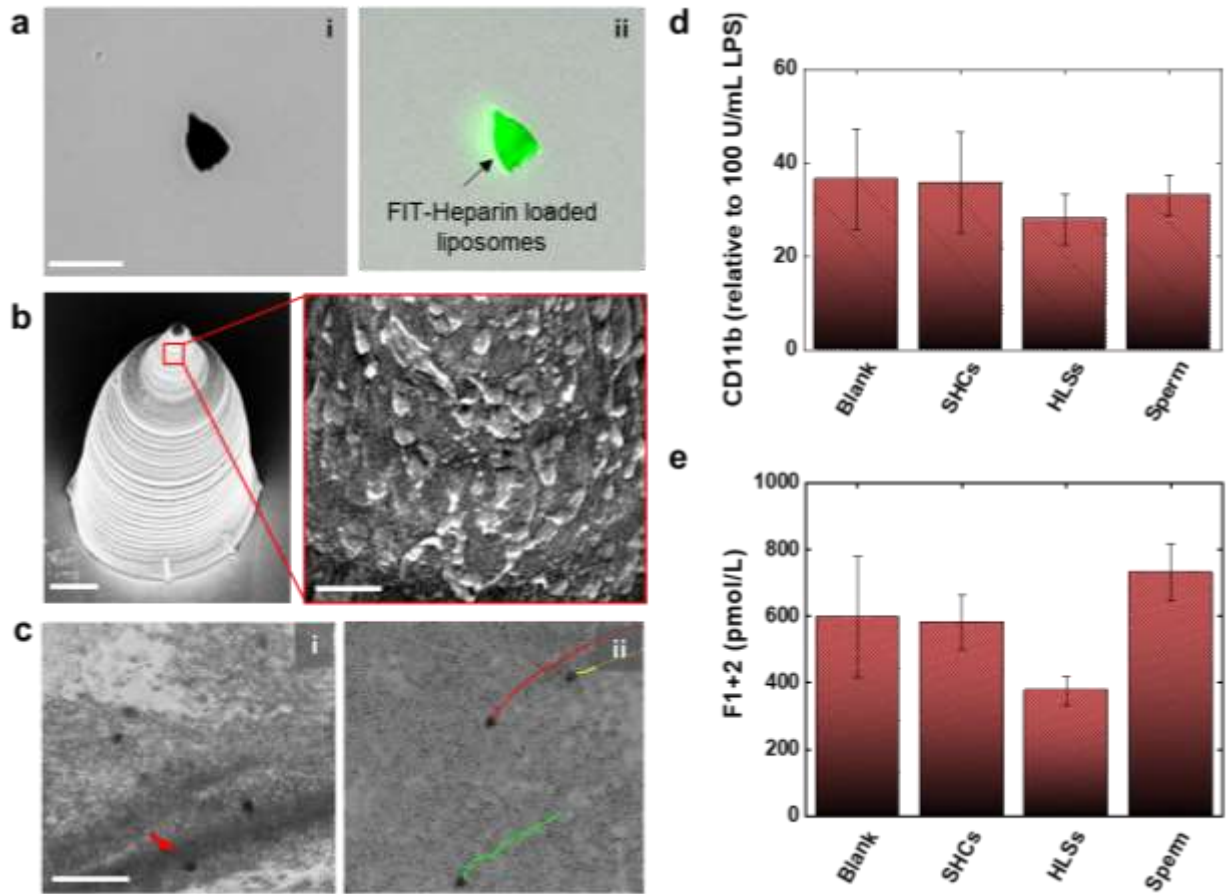
Figure 5. (a) Fluorescence microscopy images of (i) blank SHC and (ii) Alexa 488-Heparin loaded liposomes immobilized SHC. Scale bar: 20 µm. (b) SEM of SHC immobilized with Heparin-loaded liposomes. Scale bars: 3 µm in the left panel and 300 nm in the right panel with higher magnification. (c) Activated clotting of the blood treated with (i) bare SHC sperm-micromotors and (ii) HLS sperm-micromotors. Red arrow points at fibrin clot. Scale bar: 100 µm. (d) Coagulation cascade activation. (n = 6). (e) Granulocyte activation. (n = 6).

CONCLUSIONS

We developed a blood adapted sperm-micromotor which efficiently swims against blood velocity comparable to the real blood stream in human body. These streamline-horned sperm-micromotors are able to work not only as individuals, but also as swarms to execute the task of heparin cargo-delivery in flowing blood. The train-like assembly is presented as an alternative to control the applied dose by controlling the number of coupled sperm. However, the overall speed of the train-like micromotor decreases against flow due to increased drag as well as no sperm tail synchronization. Thus, further experiments need to be carried out to overcome higher blood velocities in future applications, for example by employing soft materials and optimizing their hydrodynamic and magnetic properties.

Overall, the efficient synergy of the biological and the artificial parts makes sperm-hybrid micromotors possible to operate against blood stream. As one of the most powerful microscale propellers, sperm not only generate high propulsion force, but also possess a rheotaxis/thigmotaxis swimming capability which make sperm and sperm-micromotors attractive to operate under blood stream. The streamline-horned cap is used for guidance and for functional cargo transport. Additionally, the tapered horn has the function of decreasing the energy loss by squeezing into the cells, to act as an anchor to the channel surface, allowing their motion under high pulsatile flows, and to self-assemble forming sperm-trains.

As a demonstration of the application in blood, we functionalized the microcaps with liposomes loaded with heparin as a model drug. The functionalized sperm-micromotors showed a significant anti-coagulant effect while the non-functionalized sperm-micromotors did not. In future, the

immobilized liposomes can also be equipped with thermo-sensitive shells,[57] or functional groups that activate certain coagulation factors[55] toward triggered release or specific targeting.

However, there are still remaining challenges, for instance, the propulsion force is not enough yet to overcome the flow in big arteries, where the blood velocity can reach up to 20 cm/s.[58] Instead, we can envision their application in the microvascular network, in particular in vessels like venules (ca. 0.4 mm/s), or in presence of a thrombus where the blood velocity is decreased to ca. 0.15 mm/s when there is presence of aggregated platelets, red blood cells and a mesh of cross-linked fibrin proteins. Another hurdle is the micromotor navigation in complex blood vessels which depends mainly on the propulsion mechanism, the response sensitivity of the micromotor to the external guidance, the blood velocity and the fluid viscosity. Current results prove that sperm-micromotors have powerful propulsion force against pulsating blood velocity when employing the ratchet-break mechanism ($\sim$0.833 µm/s) and that can be precisely guided by weak external magnetic fields ($<$5 mT). In order to control their location precisely, it is necessary to count with a high spatial-resolution imaging technique which allows the visualization of venules as well as of the proposed micromotors. Fortunately, our group has achieved promising results towards deep tissue and real time tracking of single microstructures, ranging from 20 to 100 µm in size, employing optoacoustic imaging.[27] Successful micromotors' tracking has been achieved underneath ca. 1 cm phantom and chicken breast tissues[27] and recently in living mice. In the next step, these sperm-hybrid micromotors will be tested in living mice in both the reproductive and circulatory systems. In a real scenario, a long-distance navigation can be performed for example by the intrinsic sperm rheotaxis which allows sperm to swim against flow and close to boundaries (natural sperm guidance mechanism towards the oocyte), to the venules instead of getting lost in the capillary

network. Then, a magnetic field can be applied for precise guidance toward the disease target when the sperm-micromotors get near to the disease site.

Regarding the safety of sperm-micromotors in future in vivo applications, we carried out experiments with ex vivo human whole blood using Chandler loops (which employs an ELISA assay). Blood incubated with sperm and microcaps were found to be not different from the bare control on the levels of coagulation and granulocyte activation indicators, demonstrating that neither specific immune response nor inflammation was induced by sperm or microcaps. Therefore, we believe that the sperm are safe to be used in blood and we expect to perform further experiments in living organisms in future.

For those diseases originating in blood, such as embolism, sperm-micromotors loaded with multiple drugs in both of the sperm and the SHC caps can be precisely guided to the disease site and efficiently enhance the local drug dose by avoiding body fluid dilution. Sperm-micromotors can be furthermore modified to treat internal hemorrhage and its related inflammation of the internal organs[60] which is unreachable from outside.

Results shown in the current manuscript not only exhibit a successful blood adapted sperm-micromotor, but also serve to identify the minimum requirements that any other medical microrobot should fulfill to be able to operate in blood vessels. Although we are aware that additional optimizations might be necessary before moving to animal trials, we believe this is the first micromotor which has satisfied most of the key needs to safely and efficiently operate in flowing blood, initiating sperm-micromotors applications in different environments from the reproductive system, due to some notorious advantages: strong sperm propulsion, sperm rheotaxis, biocompatibility, and capability of loading therapeutics in both the sperm and microcaps.

MATERIALS AND METHODS

Fabrication of microcaps. Microcaps were designed and programmed in the Describe software (Nanoscribe). The flow simulation was performed with SolidWorks, in which the relative speed between the microcaps and the flow was set as 50 µm/s. The computational domain was set as 2873 µm^3. The system was meshed with 41984 elements. In the particle studies, the impact condition between cell-mimicking particles and the microcaps was set as ideal reflection. More details can be found in **Supporting Information.** The 3D-manufacturing of the microcaps was accomplished by two-photon lithography (Nanoscribe).[37] After the microstructures were dried in a critical point drier (Autosamdri-931), highly purified Ti, Fe and SiO$_2$ (99.995%) were sequentially deposited on the microcaps by e-beam evaporation (Edwards Ebeam). For single sperm-micromotors, the microcaps were coated with 2 nm of Ti, 15 nm of Fe, another 2 nm of Ti and 10 nm of SiO$_2$. For sperm-trains, Fe was deposited with a 75° tilt so that the dipoles of all SHCs could be arranged toward the same direction under magnetization. The caps for the sperm-train assembly were also further coated with Ti and SiO$_2$ under the same conditions as the individual stream-lined caps. The magnetostatic simulation was done using SolidWorks, in which the magnetic permeability of the Fe coating, the Ti coating and the environmental fluid were set as 2.50000×10^{-1}, 1.25670×10^{-6} and 1.25662×10^{-6} H/m respectively. The resulting magnetic field intensity was calculated by solving Maxwell's equations with a fully coupled linear method. Flow profile of blood in microchannels. Channel dimension: Length (x) = 1 mm; Thickness (y) = 0.1 mm; Width (z) = 4 mm. Wall condition: real wall (no-slip); Roughness: 1 µm. Probes positions: (9, 0.008, 2); (9, 0.003, 2). Inlet: constant velocity. The streamlines of the flow and the relative pressure for both the tubular and streamlined caps is shown in **Video S13**.

Characterization of swimming performance. The microfluidic chips were designed to be 100 μm in thickness and 4 mm in width. The channel width was designed large enough for the sperm-micromotors to stay far from the channel edge in order to avoid the blood velocity difference at different horizontal positions. An SU8 master was first manufactured by maskless lithography (MLA). PDMS chips were then replicated out of the master and bound to glass sides. Sperm were dispersed in SP-TALP and purified with a swim-up method.[61] Attributed to the restriction of the optical microscopy, we were not able to clearly observe the sperm-micromotor in original undiluted blood when the light was totally blocked by an increased numbers of blood cells. Thus, the blood dilutions from 8× to 2× were prepared by directly diluting the original whole blood with relevant amounts of PBS. To simulate the real practice as closely as possible, we performed all the experiments with fresh whole blood. We found sperm-micromotors could easily get stuck in blood stored for more than 12 hours due to the blood clotting generated in *in vitro* settings, which was not found in reconstituted solutions with extracted red blood cells though. Blood velocity was introduced by a microfluidic syringe pump (neMESYS). To mimic the real application, a heating unit was used to maintain the temperature at 37°C for all experiments. An inverted microscope and a high-speed camera were used to record the swimming trajectory of the sperm-micromotors. Further analysis was done by ImageJ.

Liposomes immobilization. Unilamellar liposomes were prepared by using a mini liposome extruder (Avanti). Briefly, 1,2-distearoyl-sn-glycero-3-phosphoethanolamine (DSPE) and cholesterol at a weight ratio of 4:1 were fully mixed and dried under the protection of nitrogen flow. After that, the mixture was dispersed in heparin sodium salt (Alfa Aesar) solution at a concentration of 50 mg/mL and extruded at 60°C. The liposomes immobilization was accomplished by an improved method from the literature.[4,52,62] First, the microcaps were

carboxylated by treating them with carboxyethylsilanetriol (abcr). Then they were incubated in the liposome's solution in presence of EDC/NHS at 37°C. After that, the sample was washed with water three times and dried in a critical point drier.

Anti-coagulation test. The heparin-loaded liposomes and the HLSs were prepared as mentioned above. 200 µM of lipid concentration was used to gain a high dose of heparin. Thrombin (Sigma-Aldrich) was used to induce the blood clotting for the ACT determination and microscopy observation, respectively at concentrations of 0.2 and 1 U/mL. The sperm and microcaps were both at a concentration of 3×10^5 microcaps/mL. The ACT was determined at 37 °C following a tube method as reported in the literature.[63] The fibrin clots formation was examined every 10 s (n = 4). The whole blood incubation assay was performed by using Chandler loops as described elsewhere.[64] Sperm, SHCs and HLSs were used at a concentration of 3×10^4 of them/mL. After 2 h of incubation, without air under constant shaking, thrombin F1+2 fragment was determined with a commercial ELISA kit (Enzygnost F1+2 micro). To determine the CD11b expression level, the blood sample was stained with CD11b-PacificBlue (Biolegend) and analyzed following a lyse-no-wash protocol. The result was obtained by flow cytometry (LSR Fortessa) and further normalized to the control group, activated with 100 U/mL lipopolysaccharide.

Ethics statement. The work with human blood has been approved by the ethics committee of the Sächsische Landesärztekammer under the license "Az. EK-BR-24/18-1". Blood samples were collected with informed consent of donors. Frozen bovine sperm were purchased from Masterrind GmbH. No ethical approval was required for their use.

AUTHOR INFORMATION

Corresponding Author

Haifeng Xu

h.xu@ifw-dresden.de

Present Address

Institute for Integrative Nanosciences, IFW Dresden, Helmholtzstraße 20, 01069 Dresden

Dr. Mariana Medina Sánchez

m.medina.sanchez@ifw-dresden.de

Present Address

Institute for Integrative Nanosciences, IFW Dresden, Helmholtzstraße 20, 01069 Dresden
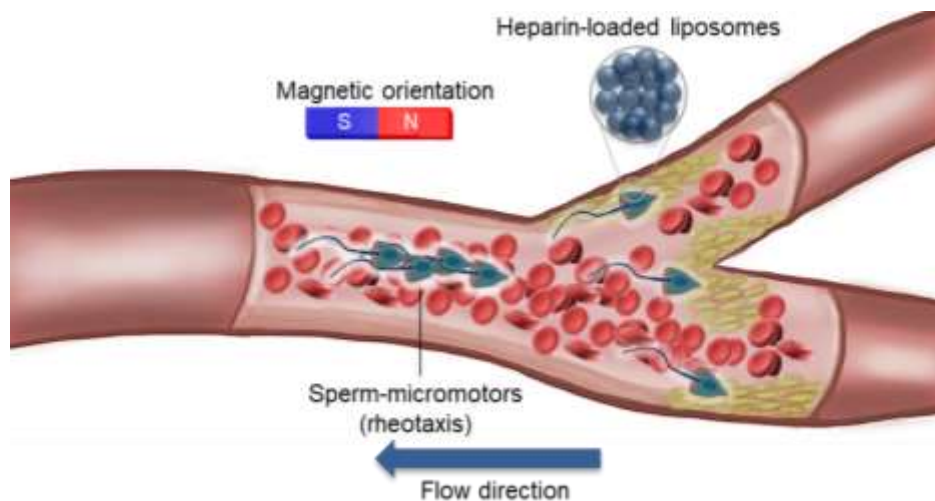
Author Contributions

H.X., M.M-S and O.G.S. conceived the project. H.X. and M.M-S designed the experiments with the help of O.G.S. H.X. performed the main part of the experimental work. M.M. and H.X. performed the whole blood incubation assay with the help of C.W. H.X. and M.M-S. wrote the manuscript. All authors commented the manuscript and figures.

TOC Image

ASSOCIATED CONTENT

The supporting information is available free of charge *via* the Internet at http://pubs.acs.org.

List of Supporting Figures:

Figure. S1. Trajectories of stream lines around the proposed sperm microcaps, related to flow velocity and pressure.

Figure. S2. Hysteresis loop of SHC sperm-micromotor speed against continuously changing blood flow.

Figure. S3. Roughness profile of the employed PDMS fluidic channel.

Figure. S4. Flow profile of blood in microchannels.

Figure. S5. Schematic of the assembling of two SHCs under magnetic field.

Figure. S6. SEM images of SHCs immobilized with different concentrations of liposomes.

List of Supporting Movies:

Video S1. Free sperm swimming in 2× diluted blood. (Real time)

Video S2. Coupling of sperm and SHCs. (4× speed)

Video S3. SHC sperm-micromotor swimming in 2× diluted blood. (Real time)

Video S4. Guidance of a SHC sperm-micromotor against flowing blood. (Real time)

Video S5. Swimming performance of SHC sperm-micromotor *versus* blood velocity. (Real time)

Video S6. SHC sperm-micromotor swimming against continuously changing blood velocity. (4× speed)

Video S7. SHC sperm-micromotor swimming against pulsing blood velocity. (2× speed)

Video S8. SHC sperm-micromotor swimming in a non-backward motion. (2× speed)

Video S9. Swimming height determination of SHC sperm-micromotors. (Speeds see labels in different sections)

Video S10. Sperm-micromotor swimming in a 1 mm thick microchannel. (Speeds see labels in different sections)

Video S11. Sperm-train transport and sperm release in sperm medium. (Speeds see labels in different sections)

Video S12. Sperm-train transport swimming in 4× diluted blood. (Speeds see labels in different sections)

Video S13. Flow simulation of microcaps in blood.

REFERENCES

(1)   Medina-Sanchez, M.; Xu, H.; Schmidt, O. G. Micro- and Nano-Motors: The New Generation of Drug Carriers. *Ther. Deliv.* **2018**, *9*, 303–316.

(2)   Solovev, A. A.; Mei, Y.; Ureña, E. B.; Huang, G.; Schmidt, O. G. Catalytic Microtubular Jet Engines Self-Propelled by Accumulated Gas Bubbles. *Small* **2009**, *5*, 1688–1692.

(3)   Zhang, L.; Abbott, J. J.; Dong, L.; Kratochvil, B. E.; Bell, D.; Nelson, B. J. Artificial Bacterial Flagella: Fabrication and Magnetic Control. *Appl. Phys. Lett.* **2009**, *94*, 64107.

(4)   Felfoul, O.; Mohammadi, M.; Taherkhani, S.; De Lanauze, D.; Xu, Y. Z.; Loghin, D.; Essa, S.; Jancik, S.; Houle, D.; Lafleur, M. Magneto-Aerotactic Bacteria Deliver Drug-Containing Nanoliposomes to Tumour Hypoxic Regions. *Nat. Nanotechnol.* **2016**, *11*, 941–947.

(5)   Solovev, A. A.; Xi, W.; Gracias, D. H.; Harazim, S. M.; Deneke, C.; Sanchez, S.; Schmidt, O. G. Self-Propelled Nanotools. *ACS Nano* **2012**, *6*, 1751–1756.

(6)   Srivastava, S. K.; Medina-Sánchez, M.; Koch, B.; Schmidt, O. G. Medibots: Dual-Action Biogenic Microdaggers for Single-Cell Surgery and Drug Release. *Adv. Mater.* **2016**, *28*, 832–837.

(7)   Wu, Z.; Troll, J.; Jeong, H.-H.; Wei, Q.; Stang, M.; Ziemssen, F.; Wang, Z.; Dong, M.; Schnichels, S.; Qiu, T.; Fischer, P. A Swarm of Slippery Micropropellers Penetrates the

Vitreous Body of the Eye. *Sci. Adv.* **2018**, *4*, eaat4388.

(8)   Ullrich, F.; Bergeles, C.; Pokki, J.; Ergeneman, O.; Erni, S.; Chatzipirpiridis, G.; Pané, S.; Framme, C.; Nelson, B. J. Mobility Experiments With Microrobots for Minimally Invasive Intraocular Surgery. *Invest. Ophthalmol. Vis. Sci.* **2013**, *54*, 2853–2863.

(9)   Morales-Narváez, E.; Guix, M.; Medina-Sánchez, M.; Mayorga-Martinez, C. C.; Merkoçi, A. Micromotor Enhanced Microarray Technology for Protein Detection. *Small* **2014**, *10*, 2542–2548.

(10)   Su, Y.; Ge, Y.; Liu, L.; Zhang, L.; Liu, M.; Sun, Y.; Zhang, H.; Dong, B. Motion-Based PH Sensing Based on the Cartridge-Case-Like Micromotor. *ACS Appl. Mater. Interfaces* **2016**, *8*, 4250–4257.

(11)   Zhao, G.; Viehrig, M.; Pumera, M. Challenges of the Movement of Catalytic Micromotors in Blood. *Lab Chip* **2013**, *13*, 1930–1936.

(12)   Soler, L.; Martínez-Cisneros, C.; Swiersy, A.; Sánchez, S.; Schmidt, O. G. Thermal Activation of Catalytic Microjets in Blood Samples Using Microfluidic Chips. *Lab Chip* **2013**, *13*, 4299–4303.

(13)   Venugopalan, P. L.; Sai, R.; Chandorkar, Y.; Basu, B.; Shivashankar, S.; Ghosh, A. Conformal Cytocompatible Ferrite Coatings Facilitate the Realization of a Nanovoyager in Human Blood. *Nano Lett.* **2014**, *14*, 1968–1975.

(14)   Baylis, J. R.; Yeon, J. H.; Thomson, M. H.; Kazerooni, A.; Wang, X.; St. John, A. E.; Lim, E. B.; Chien, D.; Lee, A.; Zhang, J. Q.; Piret, J. M.; Machan, L. S.; Burke, T. F.; White, N. J.; Kastrup, C. J. Self-Propelled Particles That Transport Cargo through Flowing Blood and Halt Hemorrhage. *Sci. Adv.* **2015**, *1*, e1500379.

(15)   Wu, Z.; Li, T.; Li, J.; Gao, W.; Xu, T.; Christianson, C.; Gao, W.; Galarnyk, M.; He, Q.;

Zhang, L. Turning Erythrocytes into Functional Micromotors. *ACS Nano* **2014**, *8*, 12041–12048.

(16) Khalil, I. S. M.; Adel, A.; Mahdy, D.; Micheal, M. M.; Mansour, M.; Hamdi, N.; Misra, S. Magnetic Localization and Control of Helical Robots for Clearing Superficial Blood Clots. *APL Bioeng.* **2019**, *3*, 26104.

(17) Sherwood, L. *Human Physiology: From Cells to Systems*; Cengage learning, 2015.

(18) Waugh, A.; Grant, A. *Ross & Wilson Anatomy and Physiology in Health and Illness E-Book*; Elsevier Health Sciences, 2014.

(19) Kolaczkowska, E.; Kubes, P. Neutrophil Recruitment and Function in Health and Inflammation. *Nat. Rev. Immunol.* **2013**, *13*, 159–175.

(20) Champion, J. A.; Walker, A.; Mitragotri, S. Role of Particle Size in Phagocytosis of Polymeric Microspheres. *Pharm. Res.* **2008**, *25*, 1815–1821.

(21) Xiang, S. D.; Scholzen, A.; Minigo, G.; David, C.; Apostolopoulos, V.; Mottram, P. L.; Plebanski, M. Pathogen Recognition and Development of Particulate Vaccines: Does Size Matter? *Methods* **2006**, *40*, 1–9.

(22) Ishimoto, K.; Gaffney, E. A. Mechanical Tuning of Mammalian Sperm Behaviour by Hyperactivation, Rheology and Substrate Adhesion: A Numerical Exploration. *J. R. Soc. Interface* **2016**, *13*, 20160633.

(23) Mei, Y.; Solovev, A. A.; Sanchez, S.; Schmidt, O. G. Rolled-Up Nanotech on Polymers: From Basic Perception to Self-Propelled Catalytic Microengines. *Chem. Soc. Rev.* **2011**, *40*, 2109–2119.

(24) Gao, W.; Pei, A.; Wang, J. Water-Driven Micromotors. *ACS Nano* **2012**, *6*, 8432–8438.

(25) Miki, K.; Clapham, D. E. Rheotaxis Guides Mammalian Sperm. *Curr. Biol.* **2013**, *23*,

443–452.

(26)   Pané, S.; Puigmartí-Luis, J.; Bergeles, C.; Chen, X. Z.; Pellicer, E.; Sort, J.; Počepcová, V.; Ferreira, A.; Nelson, B. J. Imaging Technologies for Biomedical Micro- and Nanoswimmers. *Adv. Mater. Technol.* **2019**, *4*, 1–16.

(27)   Aziz, A.; Medina-Sánchez, M.; Claussen, J.; Schmidt, O. G. Real-Time Optoacoustic Tracking of Single Moving Micro-Objects in Deep Phantom and *Ex Vivo* Tissues. *Nano Lett.* **2019**, *19*, 6612–6620.

(28)   Gur, Y.; Breitbart, H. Protein Synthesis in Sperm: Dialog between Mitochondria and Cytoplasm. *Mol Cell Endocrinol* **2008**, *282*, 45–55.

(29)   Rooney, I. A.; Oglesby, T. J.; Atkinson, J. P. Complement in Human Reproduction: Activation and Control. *Immunol Res* **1993**, *12*, 276–294.

(30)   Kelly, R. W.; Holland, P.; Skibinski, G.; Harrison, C.; McMillan, L.; Hargreave, T.; James, K. Extracellular Organelles (Prostasomes) Are Immunosuppressive Components of Human Semen. *Clin Exp Immunol* **1991**, *86*, 550–556.

(31)   Ceylan, H.; Yasa, I. C.; Yasa, O.; Tabak, A. F.; Giltinan, J.; Sitti, M. 3D-Printed Biodegradable Microswimmer for Theranostic Cargo Delivery and Release. *ACS Nano* **2019**, *13*, 3353–3362.

(32)   Suk, J. S.; Xu, Q.; Kim, N.; Hanes, J.; Ensign, L. M. PEGylation as a Strategy for Improving Nanoparticle-Based Drug and Gene Delivery. *Adv. Drug Deliv. Rev.* **2016**, *99*, 28–51.

(33)   Zhang, H.; Li, Z.; Wu, Z.; He, Q. Cancer Cell Membrane-Camouflaged Micromotor. *Adv. Ther.* **2019**, *DOI: 10.10*, 1900096(1-7).

(34)   Medina-Sánchez, M.; Schwarz, L.; Meyer, A. K.; Hebenstreit, F.; Schmidt, O. G. Cellular

Cargo Delivery: Toward Assisted Fertilization by Sperm-Carrying Micromotors. *Nano Lett.* **2016**, *16*, 555–561.

(35) Magdanz, V.; Sanchez, S.; Schmidt, O. G. Development of a Sperm-Flagella Driven Micro-Bio-Robot. *Adv. Mater.* **2013**, *25*, 6581–6588.

(36) Barkalina, N.; Jones, C.; Coward, K. Nanomedicine and Mammalian Sperm: Lessons from the Porcine Model. *Theriogenology* **2016**, *85*, 74–82.

(37) Xu, H.; Medina-Sanchez, M.; Magdanz, V.; Schwarz, L.; Hebenstreit, F.; Schmidt, O. G.; Medina-Sánchez, M.; Magdanz, V.; Schwarz, L.; Hebenstreit, F.; Schmidt, O. G. Sperm-Hybrid Micromotor for Targeted Drug Delivery. *ACS Nano* **2018**, *12*, 327–337.

(38) Xu, H.; Medina-sánchez, M.; Brison, D. R.; Edmondson, R. J.; Taylor, S. S.; Nelson, L.; Zeng, K.; Bagley, S.; Ribeiro, C.; Lina, P. R.; Lucena, E.; Schmidt, C. K.; Schmidt, O. G. Human Spermbots for Cancer-Relevant Drug Delivery. *arXiv:1904.12684* **2019**.

(39) Chen, C.; Chang, X.; Angsantikul, P.; Li, J.; Esteban-Fernández de Ávila, B.; Karshalev, E.; Liu, W.; Mou, F.; He, S.; Castillo, R.; Liang, Y.; Guan, J.; Zhang, L.; Wang, J. Chemotactic Guidance of Synthetic Organic/Inorganic Payloads Functionalized Sperm Micromotors. *Adv. Biosyst.* **2018**, *2*, 1700160.

(40) Geerts, N.; McGrath, J.; Stronk, J. N.; Vanderlick, T. K.; Huszar, G. Spermatozoa as a Transport System of Large Unilamellar Lipid Vesicles into the Oocyte. *Reprod. Biomed. Online* **2014**, *28*, 451–461.

(41) Yeh, C.; Lu, S.; Chen, Y. Microcirculation Volumetric Flow Assessment Using High-Resolution, Contrast-Assisted Images. *IEEE Trans. Ultrason. Ferroelectr. Freq. Control* **2008**, *55*, 74–83.

(42) Goldsmith, H. L.; Turitto, V. T. Rheological Aspects of Thrombosis and Haemostasis:

Basic Principles and Applications. *Thromb. Haemost.* **1986**, *56*, 415–435.

(43) Jacobs, M.; Slaaf, D. W.; Lemmens, H. A. J.; Reneman, R. S. The Use of Hemorheological and Microcirculatory Parameters in Evaluating the Effect of Treatment in Raynaud's Phenomenon. *Vasc. Surg.* **1987**, *21*, 9–16.

(44) Zhang, Z.; Liu, J.; Meriano, J.; Ru, C.; Xie, S.; Luo, J.; Sun, Y. Human Sperm Rheotaxis: A Passive Physical Process. *Sci. Rep.* **2016**, *6*, 1–8.

(45) Klindt, G. S.; Ruloff, C.; Wagner, C.; Friedrich, B. M. Load Response of the Flagellar Beat. *Phys. Rev. Lett.* **2016**, *117*, 1–5.

(46) Manning, W. J.; Katz, S. E.; Douglas, P. S.; Silverman, D. I. Atrial Ejection Force: A Noninvasive Assessment of Atrial Systolic Function. *J. Am. Coll. Cardiol.* **1993**, *22*, 221–225.

(47) Pastuszak, A. W.; Wang, R. Varicocele and Testicular Function. *Asian J. Androl.* **2015**, *17*, 659–667.

(48) Miller, J. D.; Pegelow, D. F.; Jacques, A. J.; Dempsey, J. A. Skeletal Muscle Pump *versus* Respiratory Muscle Pump: Modulation of Venous Return from the Locomotor Limb in Humans. *J. Physiol.* **2005**, *563*, 925–943.

(49) Withana, R. J.; Rodrigo, K. Significance of Dilution Errors in the Measurement of Erythrocyte Sedimentation Rate. *J. Natl. Sci. Found. Sri Lanka* **1996**, *24*.

(50) Han, K.; Shields, C. W.; Diwakar, N. M.; Bharti, B.; López, G. P.; Velev, O. D. Sequence-Encoded Colloidal Origami and Microbot Assemblies from Patchy Magnetic Cubes. *Sci. Adv.* **2017**, *3*, e1701108.

(51) Xie, H.; Sun, M.; Fan, X.; Lin, Z.; Chen, W.; Wang, L.; Dong, L.; He, Q. Reconfigurable Magnetic Microrobot Swarm: Multimode Transformation, Locomotion, and Manipulation.

Sci. Robot. **2019**, *4*, eaav8006.

(52)   Kim, J.-M.; Ji, E.-K.; Woo, S. M.; Lee, H.; Ahn, D. J. Immobilized Polydiacetylene

Vesicles on Solid Substrates for Use as Chemosensors. *Adv. Mater.* **2003**, *15*, 1118–1121.

(53)   Crowe, L. M.; Womersley, C.; Crowe, J. H.; Reid, D.; Appel, L.; Rudolph, A. Prevention

of Fusion and Leakage in Freeze-Dried Liposomes by Carbohydrates. *Biochim. Biophys.*

Acta, Biomembranes **1986**, *861*, 131–140.

(54)   Dhoot, N. O.; Wheatley, M. A. Microencapsulated Liposomes in Controlled Drug

Delivery: Strategies to Modulate Drug Release and Eliminate the Burst Effect. *J. Pharm.*

Sci. **2003**, *92*, 679–689.

(55)   Maitz, M. F.; Freudenberg, U.; Tsurkan, M. V; Fischer, M.; Beyrich, T.; Werner, C. Bio-

Responsive Polymer Hydrogels Homeostatically Regulate Blood Coagulation. *Nat.*

Commun. **2013**, *4*, 2168.

(56)   Sperling, C.; Maitz, M. F.; Talkenberger, S.; Gouzy, M.-F.; Groth, T.; Werner, C. *In Vitro*

Blood Reactivity to Hydroxylated and Non-Hydroxylated Polymer Surfaces. *Biomaterials*

2007, *28*, 3617–3625.

(57)   Chen, W.-H.; Regen, S. L. Thermally Gated Liposomes. *J. Am. Chem. Soc.* **2005**, *127*,

6538–6539.

(58)   Gabe, I. T.; Gault, J. H.; Robert, R. J.; Mason, D. T.; Mills, C. J.; Schillingford, J.;

Braunwald Eugene, E. Measurement of Instantaneous Blood Blood Flow Velocity and

Pressure in Conscious Man with a Catheter-Tip Velocity Probe. *Circulation* **1969**, *40*,

603–614.

(59)   International Commission on Non-Ionizing Radiation, (ICNIRP). Guidelines on Limits of

Exposure to Static Magnetic Fields. *Health Phys.* **2009**, *96*, 504–514.

(60)   Desai, A. U.; Saunders, M. P.; Anderson, H. J.; Howlett, D. C. Successful Transcatheter Arterial Embolisation of a Cystic Artery Pseudoaneurysm Secondary to Calculus Cholecystitis: A Case Report. *J. Radiol. Case Rep.* **2010**, *4*, 18–22.

(61)   Volpes, A.; Sammartano, F.; Rizzari, S.; Gullo, S.; Marino, A.; Allegra, A. The Pellet Swim-up Is the Best Technique for Sperm Preparation during *In Vitro* Fertilization Procedures. *J. Assist. Reprod. Genet.* **2016**, *33*, 765–770.

(62)   Mhanna, R.; Qiu, F.; Zhang, L.; Ding, Y.; Sugihara, K.; Zenobi-Wong, M.; Nelson, B. J. Artificial Bacterial Flagella for Remote-Controlled Targeted Single-Cell Drug Delivery. *Small* **2014**, *10*, 1953–1957.

(63)   Hattersley, P. G. Activated Coagulation Time of Whole Blood. *Jama* **1966**, *196*, 436–440.

(64)   Maitz, M. F.; Sperling, C.; Wongpinyochit, T.; Herklotz, M.; Werner, C.; Seib, F. P. Biocompatibility Assessment of Silk Nanoparticles: Hemocompatibility and Internalization by Human Blood Cells. *Nanomedicine Nanotechnology, Biol. Med.* **2017**, *13*, 2633–2642.